

# Journal of Biomedical Optics

BiomedicalOptics.SPIEDigitalLibrary.org

## **Feasibility study on photoacoustic guidance for high-intensity focused ultrasound-induced hemostasis**

Van Phuc Nguyen  
Jeehyun Kim  
Kang-lyeol Ha  
Junghwan Oh  
Hyun Wook Kang

# Feasibility study on photoacoustic guidance for high-intensity focused ultrasound-induced hemostasis

Van Phuc Nguyen,<sup>a</sup> Jeehyun Kim,<sup>b</sup> Kang-lyeol Ha,<sup>c</sup> Junghwan Oh,<sup>a,d</sup> and Hyun Wook Kang<sup>a,d,\*</sup>

<sup>a</sup>Pukyong National University, Interdisciplinary Program of Marine-Bio, Department of Electrical and Mechanical Engineering, 45 Yongso-ro, Nam-Gu, Busan 608-737, Republic of Korea

<sup>b</sup>Kyungpook National University, School of Electrical Engineering and Computer Science, 80 Daehakro, Bukgu, Daegu 702-701, Republic of Korea

<sup>c</sup>Pukyong National University, Department of Physics, 45 Yongso-ro, Nam-Gu, Busan 608-737, Republic of Korea

<sup>d</sup>Pukyong National University, Center for Marine-Integrated Biomedical Technology (BK 21 Plus), Department of Biomedical Engineering, 45 Yongso-ro, Nam-Gu, Busan 608-737, Republic of Korea

**Abstract.** The feasibility of photoacoustic imaging (PAI) application was evaluated to map punctured blood vessels thermally treated by high-intensity focused ultrasound (HIFU) for hemostasis. A single-element HIFU transducer with a central frequency of 2.0 MHz, was used to induce thermal hemostasis on the punctured arteries. The HIFU-treated lesion was imaged and localized by high-contrast PAI guidance. The results showed that complete hemostasis was achieved after treatment of the damaged blood vessels within 25 to 52 s at the acoustic intensity of 3600 W/cm<sup>2</sup>. The coagulation time for the animal artery was ~20% longer than that of the phantom possibly due to a lower Young's modulus. The reconstructed PA images were able to distinguish the treated area from the surrounding tissue in terms of augmented signal amplitudes (up to three times). Spectroscopic studies demonstrated that the optimal imaging wavelength was found to be 700 nm in order to reconstruct high-contrast photoacoustic images on HIFU-treated lesions. The proposed PAI integrated with HIFU treatment can be a feasible application to obtain safe and rapid hemostasis for acute arterial bleeding.

© 2014 Society of Photo-Optical Instrumentation Engineers (SPIE) [DOI: [10.1117/1.JBO.19.10.105010](https://doi.org/10.1117/1.JBO.19.10.105010)]

Keywords: high-intensity focused ultrasound; photoacoustic imaging; hemostasis; coagulation; laser.

Paper 140350PRR received Jun. 4, 2014; revised manuscript received Sep. 15, 2014; accepted for publication Sep. 23, 2014; published online Oct. 29, 2014.

## 1 Introduction

For a few decades, a variety of investigations on bleeding control (i.e., hemostasis) methods have clinically been performed with clamping, suturing, and therapeutic devices such as laser coagulation, plasma argon, etc.<sup>1,2</sup> The primary purpose of these devices is to achieve rapid hemostasis with less complication. However, these methods have still been performed in an invasive manner (i.e., open surgery) and can hardly treat the damaged internal organs that are deeply located in a body. In particular, no clamping can be accessible to damaged tissue components in microsized such as the carotid artery, veins, and nerves.<sup>3</sup> Additionally, the current treatment approaches can merely entail superficial treatments on damaged areas with minimal coagulation in an axial direction.

Recently, high-intensity focused ultrasound (HIFU) has been investigated as a noninvasive or minimally invasive thermal therapeutic method to control acute hemorrhage and to treat tumors deeply located inside the body.<sup>4-7</sup> Ultrasound-induced tissue coagulation is a technique that can obtain hemostasis in an almost noninvasive manner without excessive heating and adverse ion radiation effect on adjacent tissue, which were often observed in laser or argon plasma applications. In previous studies on acute hemorrhage control, HIFU was used to induce the rapid temperature increase within the focused acoustic field, leading to irreversible tissue coagulation and cell necrosis in the treated region and achieving hemostasis for the targeted

tissues.<sup>8,9</sup> Due to relatively lower acoustic intensities, the peripheral area around the targeted lesions could still remain less damaged or undamaged. HIFU technology has also been applied to a large number of benign and malign solid tumors such as prostate cancer, liver, kidney, bone, and brain as well as dissolution for ischemic stroke.<sup>10-12</sup> Specifically, HIFU technique could control hemostasis for severely damaged blood vessels, eventually reducing the risk of hemorrhage and treatment.<sup>13</sup>

In order to improve the efficacy of HIFU treatment and to precisely deliver acoustic energy to the targeted lesion, the treatment procedure still needs to be monitored and evaluated in real time. Lately, HIFU treatment has been carried out with imaging guidance modalities such as magnetic resonance imaging (MRI) and ultrasound imaging.<sup>14,15</sup> However, MRI scanners are still expensive and bulky systems with lengthy scanning time. Ultrasound imaging systems are relatively cost-effective and able to readily locate the injured tissue as well as to obtain faster hemostasis than visual inspection (i.e., 25 s for Doppler ultrasound guidance versus 125 s for visual inspection).<sup>5,16</sup> However, ultrasound imaging still suffers from the lack of accuracy and specificity as well as low image contrast particularly for noninvasive localization and treatment evaluation.<sup>17</sup> Thus, to overcome the limitations of the current imaging systems, a photoacoustic imaging (PAI) approach can be used as an alternative imaging guidance modality to monitor and evaluate the process of thermal therapeutics. PAI is a nonionizing,

\*Address all correspondence to: Hyun Wook Kang, E-mail: [wkang@pknu.ac.kr](mailto:wkang@pknu.ac.kr)

noninvasive, cost-effective, and hybrid imaging technique that can provide high optical absorption with high ultrasound resolution.<sup>18,19</sup> Additionally, PAI imaging is capable of generating structural information of hemoglobin or melanin as well as functional information such as total hemoglobin concentration or blood flow with strong contrast and high spatial resolution.<sup>20,21</sup> Compared to conventional imaging modalities, the primary advantage of PAI is to image the targeted tissue in more than 5 cm depth along with spatial resolutions from 2 to 500  $\mu\text{m}$ <sup>22,23</sup> and to monitor the temperature profile in the thermal lesion generated by HIFU.<sup>24</sup> Therefore, the integration of high-contrast PAI with HIFU therapy can be a feasible image-guided tool to facilitate acute hemostasis in clinical applications.

In this study, the feasibility of HIFU application was investigated in terms of treating acute hemorrhage in tissue and incorporating high-contrast PAI guidance in order to accurately localize the treated lesions after HIFU application and thus to minimize undesirable thermal injury. Acoustic fields of the HIFU transducer in water and its thermal effects on tissue were initially characterized with a hydrophone and thermocouple. The temporal development of the coagulation process was measured and evaluated as a function of acoustic intensity in phantom and animal tissues. After HIFU treatments, histological analysis was performed and compared with photoacoustic (PA) images on the targeted tissue.

## 2 Materials and Methods

### 2.1 Tissue Samples

Two groups of samples were used for HIFU-induced hemostasis testing: phantom ( $N = 25$ ) and animal femoral arteries ( $N = 5$ ). The phantom arteries used plastic tubes of an outer diameter of 2 mm, and the animal ones (i.e., outer diameter of up to 2 mm) along with heparinized blood samples were procured from chickens at a local slaughter house. Prior to the experiments, an incision hole of  $\sim 0.5$  mm in diameter was punctured with a needle on each artery sample to induce bleeding during thermal hemostasis testing. A syringe pump (55-5920, Harvard Apparatus, Holliston, Massachusetts) was used to perfuse

blood through each sample at a constant flow rate of 20 ml/h in order to mimic physiological conditions. At the onset of bleeding through the hole, high ultrasonic energy was immediately applied to the bleeder until the hole was covered with coagulated blood (i.e., coagulum) due to thermal denaturation. The complete hemostasis was confirmed in light of no leakage throughout the artery sample as well as visual observation. In turn, the time for completion of hemostasis, termed as coagulation time in this study, was evaluated under various conditions. During HIFU application, each sample was immersed in a water bath at 38°C similar to *in vivo* environments. Degassed water was used to prevent any cavitation in the bath and to provide the impedance matching between HIFU transducer and target tissue. In the case of animal tissue testing, each post-HIFU treated tissue was imaged with a digital microscope (1.3 M Dino-Lite pro, Anmo Electronics, New Taipei City, Taiwan) to evaluate any collateral damage to the surrounding tissue. From the captured images, the extent of the thermally denatured lesion was circumferentially measured ( $N = 5$ ) with imaging software (Image J, National Institutes of Health, Bethesda, Maryland). In addition, histological analysis was post-experimentally performed to confirm hemostatic responses of the targeted tissue. The tested blood vessel samples were fixed in 10% formalin prior to standard hematoxylin & eosin (H&E) staining. Each sample was cut into a thickness of 4  $\mu\text{m}$  at the center of the HIFU-treated area, and high resolution (100 $\times$ ) digital images of the cross-sectioned tissues were captured with a Leica microscope system (Leica DM 500, New York Microscope Company, Hicksville, New York).

### 2.2 HIFU Application

Figure 1 depicts a schematic diagram of experimental setups for HIFU-induced hemostasis. A piezoelectric HIFU transducer (H-148, Sonic Concept, Woodinville, Washington) with a focal length of 51.7 mm yielded ultrasound waves at a central frequency of 2.0 MHz. Continuous ultrasound waves were generated with a function generator (DDF 3010, Shanghai MCP, Shanghai, China) and then amplified by an RF amplifier (525LA, ENI, Rochester, New York). A blood-perfused sample

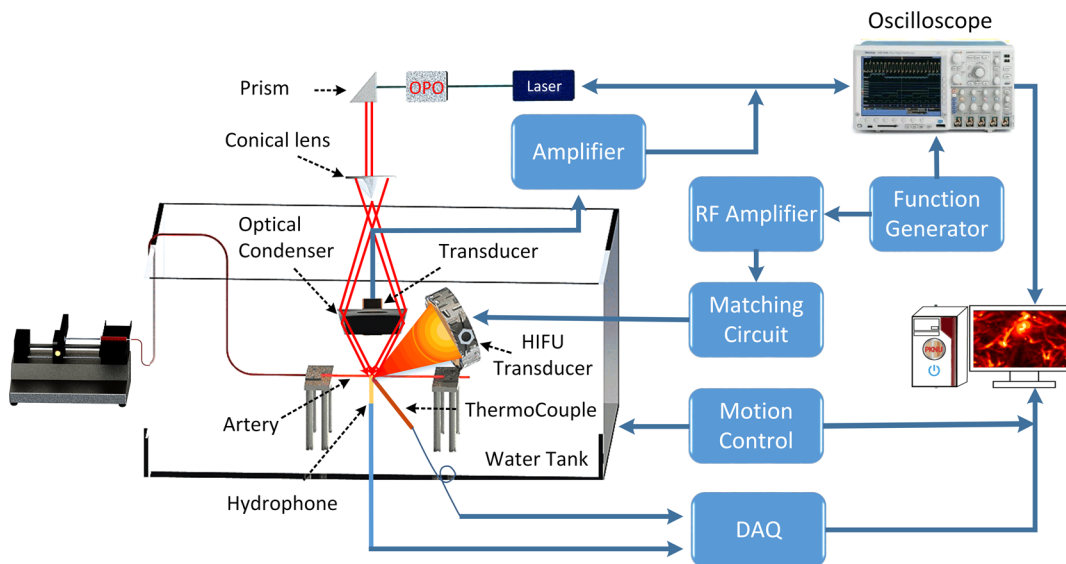


**Fig. 1** Experimental setup of high-intensity focused ultrasound (HIFU)-induced thermal coagulation on artery with assistance of photoacoustic imaging (PAI).

was positioned underneath the transducer and then exposed to focused acoustic fields. The HIFU transducer was immersed in a water tank with the beam axis directed toward an incision hole to yield acoustic fields within a sample. In order to achieve the precise position of a focal spot, a three-dimensional plastic conical cap was designed, fabricated, and mounted on the HIFU transducer. In turn, the focus of the transducer was simply aligned with the location of the targeted hole. For phantom experiments, the acoustic intensities at the focus ranged from 1100 to 4600 W/cm<sup>2</sup> to identify the appropriate dosage for HIFU treatment on animal tissue. Coagulation time, defined as the time required for complete hemostasis, was measured and compared as a function of acoustic intensity ( $N = 5$  per condition). Based upon the phantom results, the acoustic intensity of 3600 W/cm<sup>2</sup> was then selected and used for animal artery experiments due to potentially rapid coagulation along with minimal thermal injury. Additionally, the peak temperature variations at the focus were monitored by a thermocouple (GT307, Gilwoo Company, Seoul, Republic of Korea) to identify any correlation with the measured coagulation times. Student's  $t$ -tests were performed for statistical analysis and  $p$ -value  $<0.05$  represents a statistically significant difference.

Prior to *ex vivo* tissue experiments, a HIFU transducer was evaluated in terms of spatial distribution and intensity of acoustic fields. A 0.3-mm (in diameter) needle hydrophone (Precision Acoustics, Dorset, United Kingdom) was positioned at the center of the HIFU transducer to measure pressure waveforms. The output signals were recorded and converted into acoustic parameters (i.e., acoustic pressure and intensity). The free-field acoustic pressure at the focal point measured by the hydrophone was calculated as follows:

$$p(t) = \frac{V(t)}{\mu}, \quad (1)$$

where  $p(t)$  (MPa) is the temporal acoustic pressure,  $V(t)$  (mV) is the voltage generated by the acoustic pressure incident on the active element of the hydrophone, and  $\mu$  (mV/MPa) is the hydrophone sensitivity at the acoustic working frequency. The acoustic intensity at the focal point was then estimated as follows:

$$I = \frac{P_{\text{eff}}^2}{\rho c}, \quad (2)$$

where  $P_{\text{eff}}$  is the effective value of  $p(t)$ . In addition to the hydrophone measurements, a Schlieren system was employed to qualitatively visualize the two-dimensional (2-D) beam shape of the HIFU transducer near the focal point and to compare it with the results obtained by the needle hydrophone. The detailed experimental setup of Schlieren imaging has been introduced elsewhere.<sup>25</sup>

### 2.3 Photoacoustic Imaging

To validate coagulated lesions after thermal treatment with HIFU, all the treated samples were imaged with a PAI system. Figure 1 illustrates a schematic diagram of the PAI system used for 2-D imaging. As a light source, a tunable ( $\lambda = 680$  to 2500 nm) OPO laser (Surlite OPO Plus, San Jose, California) was used and pumped by a Q-switched Nd:YAG (Surelite II, Continuum, San Jose, California) laser with a pulse duration of 5 ns at 10 Hz. In brief, the laser light from OPO was

perpendicularly reflected at the prism and then spread through a spherical conical lens, resulting in the ring-shaped pattern. The ring-shaped light was propagated through a custom-built optical condenser and was focused onto an artery sample. Upon laser irradiation, each specimen induced the PA signals, which were detected by a spherically focused single-element 5.0 MHz ultrasound transducer (V308, Panametrics, Waltham, Massachusetts) with a focal length of 2.54 cm. In order to reduce the attenuation of acoustic fields, a targeted sample was immersed in a degassed water container, and undesirable air bubbles were removed before conducting PAI. The laser beam was coaligned with the focal spot of an imaging ultrasound transducer in degassed water, and for 2-D imaging, each sample in the tissue holder was moved along  $x$ - and  $y$ -directions on a 2-D translation stage. The received PA signals were filtered and amplified by a low-noise amplifier (5072 PR, Olympus, Waltham, Massachusetts), which in turn, were converted into digital signals and recorded by a digital oscilloscope (TDS 5040, Tektronix, Beaverton, Oregon). The recorded data were used to reconstruct 2-D images of the HIFU-treated artery samples. The axial and transverse resolutions of the current PAI system were 144 and 590  $\mu\text{m}$ , respectively. All the reconstructed images were used to estimate image contrast, defined as the difference between the color of the coagulated area and its background. Thus, the contrast was determined by fractional variations in the mean signal amplitudes extracted from regions of interest (ROI) as follows:<sup>26</sup>

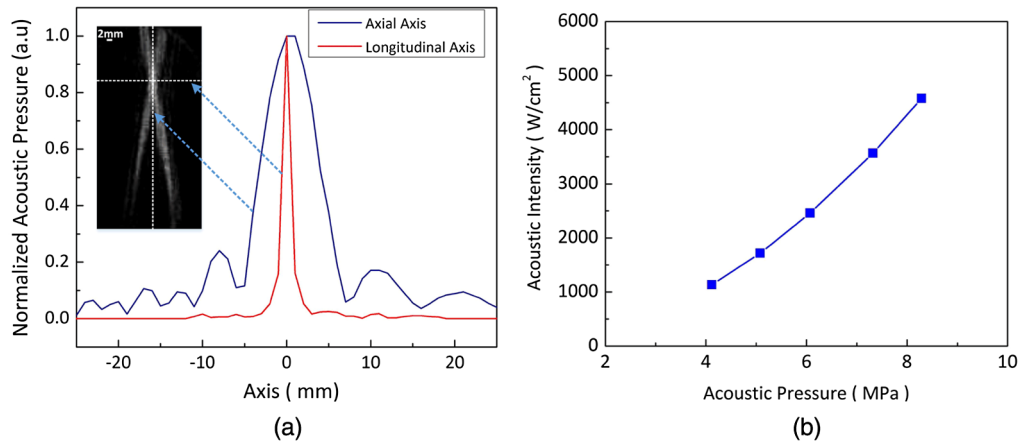
$$\text{Contrast} = \frac{\bar{A}_{\text{CB}} - \bar{A}_{\text{BG}}}{\bar{A}_{\text{BG}}}, \quad (3)$$

where  $\bar{A}_{\text{CB}}$  and  $\bar{A}_{\text{BG}}$  are the mean signal amplitudes from the coagulated blood and adjacent background, respectively. Due to functional limitations of the current laser system, near-IR wavelengths (i.e., from 700 to 900 nm with an increment of 50 nm) were merely employed for PAI and tested on the thermally treated samples to identify the spectroscopic effects of wavelength on image reconstruction and tissue differentiation.

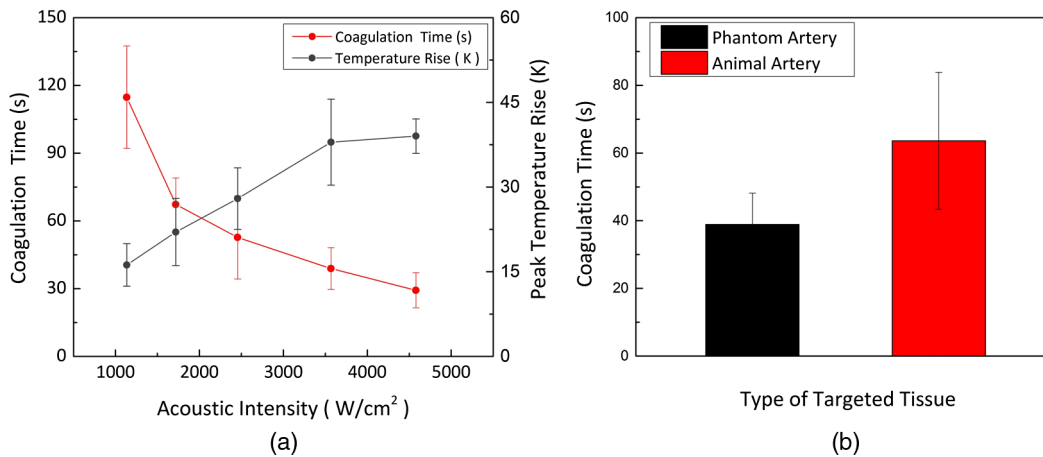
## 3 Results

Figure 2(a) illustrates characterization of the focused ultrasound waves produced by an HIFU transducer. Both axial (blue line) and longitudinal (red line) distributions of the normalized acoustic field were measured with a hydrophone as a function of radial distance. According to Fig. 3(a), the transducer generated a focal spot in an elliptical shape (i.e., 10 mm in axial and 2 mm in lateral). The Schlieren image [i.e., inset in Fig. 2(a)] also confirmed the elliptical HIFU beam at the focus shown as an intersecting point between two white dotted lines. In the Schlieren image, vertical and horizontal lines represented the axial and longitudinal axes, respectively. The corresponding acoustic intensity of the HIFU transducer was also estimated and plotted as a function of acoustic pressure used in the current experiments [Fig. 2(b)]. The intensity increased almost linearly with the applied pressure, ranging from 1100 to 4600 W/cm<sup>2</sup>.

Figure 3 represents the temporal response of complete thermal hemostasis with HIFU in phantom and animal artery samples. Both coagulation time and peak temperature rise were measured with the phantom samples at various acoustic intensities [Fig. 3(a)]. HIFU exposure was implemented on a total of 25 samples ( $N = 5$  per acoustic intensity), and all of the bleeders successfully experienced complete hemostasis. At the lowest acoustic intensity of 1100 W/cm<sup>2</sup>, the thermal coagulation time



**Fig. 2** Characterization of focused ultrasound waves: (a) normalized acoustic pressure in axial (blue)/longitudinal (red) axes and corresponding Schlieren image (inlet) and (b) acoustic intensity as function of acoustic pressure.



**Fig. 3** Quantitative evaluations on HIFU treatment on targeted artery: (a) coagulation time (red) and temperature rise (black) from phantom artery at various acoustic intensities and (b) comparison of coagulation time between phantom and animal arteries ( $I = 3600 \text{ W/cm}^2$ ).

was estimated to be almost 2 min and substantially decreased with increasing intensity down to  $\sim 30$  s. On the other hand, the temperature rise ( $\Delta T$ ) was initially around 16 K and linearly increased up to 38 K (at  $3600 \text{ W/cm}^2$ ), becoming almost saturated afterwards (i.e.,  $\Delta T \approx 40 \text{ K}$ ;  $p$ -value = 0.35). Figure 3(b) compares the complete coagulation times between phantom and

animal blood vessels at the acoustic intensity of  $3600 \text{ W/cm}^2$ . The percent difference between the two samples was  $\sim 24\%$ , indicating that almost 160% slower hemostasis occurred with the animal sample in comparison with the phantom (i.e.,  $40 \pm 10$  s for phantom artery versus  $64 \pm 20$  s for animal artery).

In order to explore the efficacy of HIFU treatment on animal artery, histological analysis stained with H&E was performed as shown in Fig. 4. A control image [Fig. 4(a)] shows a cross-sectional area of the animal blood vessel without any punctured lesion. Figure 4(b) demonstrates that the puncture was initially made at 7 o'clock in the blood vessel area and thermally treated with HIFU at  $3600 \text{ W/cm}^2$  for 52 s. From the region of interest, the punctured vessel wall was sealed by coagulum, which extruded through the media and adventitia and partially covered the outer surface of the artery. Thus, the histology image in Fig. 4(b) confirmed that the complete hemostasis was achieved with the HIFU thermal treatment.

Figure 5 exhibits top-view images of coagulated artery samples after HIFU treatment. A dotted circle indicated the position of the HIFU-treated area on the phantom artery at the acoustic intensity of  $3600 \text{ W/cm}^2$  for 40 s [Fig. 5(a)]. The incision hole was sealed with blood coagulum (i.e., black color inside the

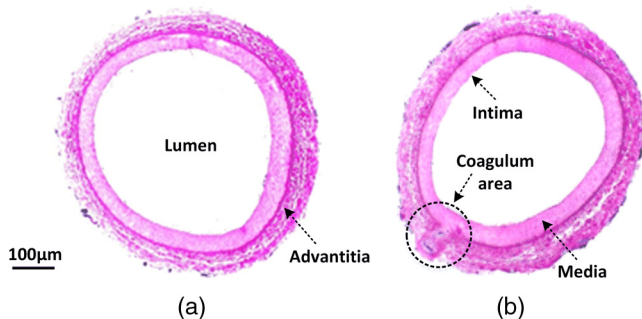


**Fig. 4** Histological images of animal artery (H&E staining; 100 $\times$ ): (a) control tissue and (b) HIFU-treated animal artery. Note that a black dotted circle indicates the position of punctured artery sealed by thermally-induced coagulum (52 s at  $3600 \text{ W/cm}^2$ ).

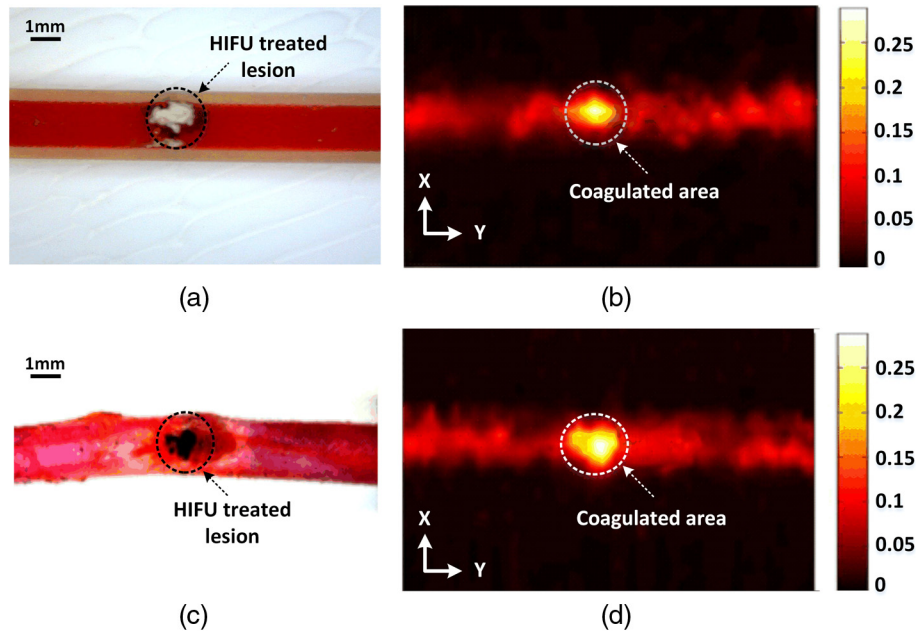


**Fig. 5** PAI mapping of tissues after HIFU coagulation: photographs of (a) phantom and (c) animal arteries ( $I = 3600 \text{ W/cm}^2$ ) and corresponding PA images of (b) phantom and (d) animal arteries acquired at 700 nm wavelength.

sample) and whitish surface discoloration (i.e., on the sample surface) after thermal treatment, which eventually prevented additional bleeding from the punctured sample. Figure 5(b) presents a PA image of the same sample in Fig. 5(a) taken by a PAI system ( $\lambda = 700 \text{ nm}$ ) after the complete hemostasis. The coagulated region in a white dotted circle demonstrated a two times higher contrast in the amplitude of PA signals as the untreated region along with a signal-to-noise ratio (SNR) of 4 dB. It was confirmed that the thickness of the sample in Fig. 5(b) was equivalent to that of the sample in Fig. 5(a). Figure 5(c) shows the HIFU-treated animal artery at the acoustic intensity of  $3600 \text{ W/cm}^2$  for 52 s. The lesion (i.e., 1 mm in diameter) in a black dotted circle evidenced the complete thermal hemostasis, covering the artery surface with black

coagulum. Based upon the acquired images, the extent of coagulative necrosis in the peripheral area was found to be  $0.5 \pm 0.2 \text{ mm}$ . In Fig. 5(d), a PA image of the same animal artery was taken at the 700-nm wavelength. Similarly to Fig. 5(b), the coagulated area showed distinctively higher contrast in the blood vessel image. Both sample images in Figs. 5(c) and 5(d) represented the equivalent sample thickness of 2 mm.

To quantitatively characterize a PA image of HIFU-treated animal artery in Fig. 5(d), the PA maximum amplitude projection at three different locations in the image was measured and compared for characteristics such as background, blood vessel, and coagulated regions as shown in Fig. 6(a) (i.e.,  $0.228 \pm 0.031$  for coagulated region versus  $0.006 \pm 0.001$  for background and  $0.095 \pm 0.013$  for blood vessel). Due to significant contrast

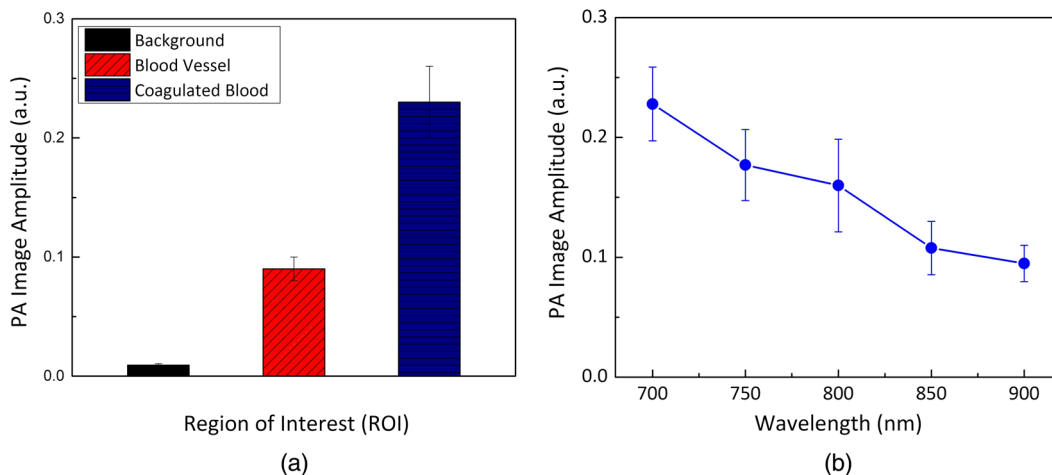


**Fig. 6** Quantitative characterization of PA image: (a) comparison of PA image contrasts acquired at 700 nm and (b) spectroscopic evaluation on PA signal amplitudes.

variations, PAI was able to differentiate the HIFU-induced coagulation area from background and other untreated areas. The image contrast from the coagulated region showed approximately 37 and 1.4 times higher than those from the background and blood vessel, respectively. To further identify the optimal PAI wavelength for precisely detecting thermally coagulated lesions after HIFU treatment, the PA amplitudes of the coagulated areas in the animal arteries were measured and compared at various incident laser wavelengths (from 700 to 900 nm by 50 nm increment). All the tissue samples were treated at the acoustic intensity of 3600 W/cm<sup>2</sup> for 52 s. Apparently, the spectroscopic measurements showed that the wavelength of 700 nm achieved the maximum light absorption by the coagulated area [Fig. 6(b)] in comparison with other wavelengths. Beyond 700 nm, the PA amplitude significantly decreased with the wavelength.

#### 4 Discussion

The current study presented the feasibility of a noninvasive HIFU therapeutic method for complete hemostasis in both phantom and animal arteries. Typically, blood coagulation requires a temperature increase up to 343 K induced by physical interactions of acoustic energy with soft tissues.<sup>8</sup> Similarly, high-acoustic intensity rapidly localized and increased the temperature (up to  $\Delta T = 38$  K within 30 s at 4600 W/cm<sup>2</sup>) within the focal point in tissue as shown in Fig. 3(a). Thus, the relatively faster temperature development eventually resulted in more efficient hemostasis in the phantom and animal blood vessels. Evidently, the temperature increase is linearly associated with the applied acoustic intensity as well as tissue properties (acoustic and thermal) as follows:<sup>27</sup>

$$\Delta T = \frac{2\alpha}{\rho c} I, \quad (4)$$

where  $\alpha$  (dB/m) is the acoustic absorption coefficient at the center frequency. Then, given the properties for the blood sample (i.e.,  $\rho = 1060$  kg/cm<sup>3</sup> and  $\alpha = 3$  dB/m),<sup>28</sup> the estimated temperature rises at 1100 and 1700 W/cm<sup>2</sup> can be  $\sim 17$  and 26 K, respectively; accordingly, the theoretical values showed a good agreement with the temperature increase measured in the current study as shown in Fig. 3(a). However, at the higher acoustic intensities (i.e., 3600 and 4600 W/cm<sup>2</sup>), the temperature increase became saturated at  $\Delta T \approx 40$  K. The saturation behavior could be primarily associated with the thermal insulation effect of the solidified coagulum on the punctured site. Once thermal denaturation was initiated, coagulum could begin to form throughout the phase change and eventually cover the bleeding area. Upon complete hemostasis, the most thermal energy would be deposited in the generated coagulum, entailing the formation of multiple microbubbles on the target surface, which was reported by Clarke et al.<sup>29</sup> According to their study, the aggregation of microbubbles would result in the formation of an acoustic barrier to the ultrasound beam on the target surface. Then, most of the incident acoustic energy could be scattered and/or partially absorbed by the bubble layer to entail inefficient energy coupling. As the temperature underneath the barrier would start to decrease due to the increased attenuation, a thermocouple would be able to merely measure the temperature change beneath the coagulated area up to  $\Delta T \approx 40$  K. Thus, it is conceived that the saturation behavior occurred due to the consequent temperature decrease by the surface bubble barrier

during HIFU thermal therapy. In fact, the current study was able to observe the generation of a group of macrobubbles on the coagulum surface during the HIFU treatment. Accordingly, the acoustic intensity of 3600 W/cm<sup>2</sup> might be the threshold intensity to obtain complete hemostasis under the current conditions. Further studies will perform temperature measurements at various points in tissue to map the spatial distribution of thermal energy and to identify the optimal acoustic intensity for rapid coagulation.

Post-experimental measurements confirmed the significant extent of collateral injury of  $0.5 \pm 0.2$  mm. It is conceivable that the thermal injury could result from both spatial and temporal effects of HIFU treatments. Compared to the diameter of the punctured hole, the HIFU beam was relatively larger (i.e., 10 by 2 mm in Fig. 2), which could have covered even the healthy tissue regions. However, there was a trade-off between collateral damage and completion of hemostasis. According to our preliminary studies, complete coagulation was difficult to achieve with the smaller size of the HIFU beam due to higher light intensity along with concentrated temperature increase as well as limited beam alignments. Particularly, the accurate positioning of the smaller beam size on the targeted tissue area extensively prolonged the entire testing time. Thus, the wider distribution of the HIFU beam was more applicable and practical to readily accomplish complete hemostasis as well as fast beam alignments in spite of the inevitably considerable thermal injury.

The current study found that the complete hemostasis required a significant amount of treatment time (i.e.,  $64 \pm 20$  s) for animal tissue. Based upon the treatment time, the spatial extent of heat diffusion could roughly be calculated to be 3 mm by using the following equation:<sup>30</sup>

$$z_{\text{therm}} = \sqrt{4 \cdot \alpha \cdot t}, \quad (5)$$

where  $z_{\text{therm}}$  (m) is the time-dependent thermal penetration depth,  $\alpha$  (m<sup>2</sup>/s) is the thermal diffusivity (e.g.,  $14 \times 10^{-7}$  m<sup>2</sup>/s for soft tissue), and  $t$  (s) is the heat accumulation time. However, it should be noted that the theoretical depth was six times thicker than that measured in the current study (i.e.,  $0.5 \pm 0.2$  mm). The thinner coagulative necrosis was conceivably associated with convective heat transfer due to blood perfusion at 20 ml/h and the degassed water environment maintained at 38°C. Vaezy et al. reported that a significant amount of heat was carried downstream during HIFU application, consequently protecting the blood vessel wall from thermal injury and simultaneously protracting the thermal treatment time to reach the targeted temperature.<sup>31</sup> Therefore, additional quantitative investigations with animal tissue are still necessary to identify the optimal treatment dose and conditions in light of beam size, coagulation time, and minimal degree of thermal injury. In an effort to evaluate the thermal treatment time,  $\Delta t$  (s), required for complete hemostasis of tissue, the Arrhenius rate equation was also used as follows:<sup>32</sup>

$$\Delta t \approx \Omega \times e^{\Lambda \cdot (T_c - T_0) / T_c}, \quad (6)$$

where  $\Omega$  is the Arrhenius integral,  $\Lambda$  is the rate constant (i.e., 244.8 for blood flow),  $T_c$  is the critical temperature (i.e., 327.7 K for microvascular blood flow), and  $T_0$  is the coagulation temperature (i.e., 323.15 K).<sup>32</sup> Since thermal coagulation is associated with irreversible conformational changes in blood (i.e.,  $\Omega = 1$ ), the estimated heating interval can be calculated

to be 62.4 s, which is comparable to the experimentally measured time (i.e.,  $64 \pm 20$  s). However, the current study defined the coagulation time as the moment when hemostasis was achieved through visual inspection. Both post-experimental histology analysis and PAI imaging merely confirmed coagulation with  $\Omega \geq 1$ . Accordingly, further information on the temperature–time relation during coagulation will be required in order to precisely assess the initiation of coagulation events and to validate the end-point of HIFU treatment.

Figure 3(b) exhibited that the coagulation time measured for animal artery was 160% longer than that for the phantom one at  $3600 \text{ W/cm}^2$  (i.e.,  $64 \pm 20$  s for animal artery versus  $40 \pm 10$  s for phantom artery). It should be noted that the phantom artery made of silicon has an order of Young's modulus higher than that of animal tissue (i.e., 2.07 MPa for phantom artery<sup>33</sup> versus 0.19 MPa for animal tissue).<sup>34</sup> In fact, the hole in the phantom artery was often deformed and became a  $<0.5$ -mm wide, elongated cut whereas the animal artery almost maintained the original shape of the needle-drilled hole. Accordingly, the geometrically altered hole in the phantom artery could have been instrumental in facilitating the thermal coagulation process during HIFU treatment. Moreover, since the wall of the animal blood vessel was less uniform and thinner than that of the phantom tube (i.e., 1 mm for phantom artery versus  $\leq 0.5$  mm for animal artery), structural differences could have contributed to the longer coagulation time owing to the relatively shorter pathway of coagulation along the incised hole.

The acquired PA images in Fig. 5 demonstrated that thermal lesions were well defined with higher contrast, compared to the surrounding areas. Image contrast typically represents the amplitude of the acquired PA signal, which is related to the optical energy locally absorbed by tissue chromophores (i.e., oxygenated hemoglobin of blood and water). Thus, the enhanced contrast indicated strong light absorption by the volumetric tissue specifically exposed to HIFU (Fig. 5). Besides, the increased PA amplitudes acquired from the HIFU-treated lesions agreed well with the findings from the previous study.<sup>35</sup> It was reported that the thermomechanical properties of tissue, expressed as a Grüneisen coefficient, could contribute to augment PA signals in coagulated tissue, in that the coefficient for coagulated blood was  $\sim 65\%$  higher than that for the native sample (i.e., 0.06 for noncoagulated and 0.09 for coagulated blood).<sup>36</sup> The Grüneisen coefficient,  $\Gamma$ , is related to the initial acoustic pressure,  $p_0$ , upon light absorption, which can be expressed as  $p_0 = \Gamma \cdot \mu_a \cdot \Phi$ , where  $\mu_a$  ( $\text{cm}^{-1}$ ) and  $\Phi$  ( $\text{J/cm}^2$ ) denote optical absorption coefficient and light fluence, respectively.<sup>37</sup> Black et al. reported that the light absorption coefficient of clotted blood was higher than one in the native state (i.e.,  $\mu_a = 8 \text{ cm}^{-1}$  for clotted blood versus  $1 \text{ cm}^{-1}$  for native blood at 700 nm).<sup>38</sup> Under the same fluence, it is conceivable that both Grüneisen and absorption coefficients can primarily determine the degree of acoustic transients as well as the quality of PA imaging. In fact, the bright areas in the acquired PA images were validated to correspond to local accumulation of solid coagulum after HIFU-induced denaturation (Fig. 5). Accordingly, the coagulated blood with the higher Grüneisen as well as optical absorption coefficients could promote stronger acoustic transients and result in more distinctive image contrast.

Spectroscopic studies on PA signal amplitudes confirmed that the degree of light absorption by thermally treated tissue at shorter optical wavelengths was higher than that at longer wavelengths due to relatively stronger PA amplitudes, which

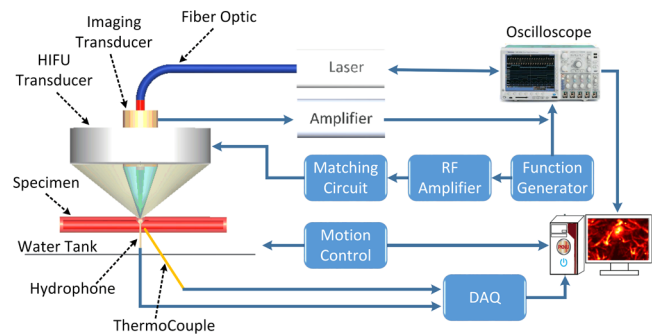


**Fig. 7** Schematic diagram of HIFU thermal treatment integrated with fiber-based PAI for real-time monitoring.

was consistent with O'Neill's report. Their study showed that the normalized PA intensity at HIFU-treated bovine muscle was 2.5 times strong at shorter wavelengths than longer wavelengths (i.e., 0.4 at 700 nm versus 0.16 at 900 nm).<sup>39</sup> It was noted that the absorption coefficients of bovine muscle were similar to those of deoxyhemoglobin between 700 and 900 nm.<sup>40,41</sup> Thus, coagulated blood could strongly absorb the incident laser light, consequently entailing higher PA contrast in reconstructed images. Furthermore, the spectroscopic PA results demonstrated the strongest PA signal amplitude measured at 700 nm [Fig. 7(b)], which possibly attributed to more light absorption specifically by the coagulated tissue. Therefore, the stronger acoustic contrast at 700 nm led up to a 90% higher SNR of 14.4 dB between coagulated blood and background, whereas 11.4, 7.9, 9.2, and 11.8 dB were estimated at 750, 800, 850, and 900 nm, respectively.

Although the current study successfully demonstrated the PAI detection of thermal lesions induced by HIFU coagulation, experimental limitations still remain for the sake of practical application. During the experiments, the coagulated areas for hemostasis were imaged with PAI followed by HIFU application due to complexities of the current system. Thus, the 2-D images hardly contained any temporal information for exhibiting the thermal coagulation process as well as capturing the moment for the complete hemostasis. A thermocouple was also used and inserted to measure the maximum temperature in the treated tissue (Fig. 1). Thus, in-depth considerations upon the integrated probes would be critical for real-time monitoring thermal treatment and precluding any postbleeding events. In fact, PAI assessment of blood coagulation can be feasible only if all the signal measurements are performed real-time and coaxially with HIFU treatment. Figure 7 shows a schematic diagram of fiber-based PAI transducers that is coaxially integrated with the HIFU transducer. Due to coalignment with the equivalent focal length, the designed transducer would readily identify the treated area as well as capture PA signals *in situ*. Presently, the follow-up studies with the combined probes are underway to identify the optimal treatment dosage, to detect the PA signals during/after HIFU treatment, to calibrate 1-D information with temperature elevation, and to acquire 2-D images as a validation tool for complete hemostasis.<sup>24</sup> The change and rate of change in PAI amplitudes will specifically be assessed and correlated to visual observation of hemostasis and histological outcome. In turn, the temperature–time relation of coagulation with PAI can reliably elucidate the relevance of PAI in determining thermal damage and its relationship to

hemostasis, given the data of blood and blood vessel for the Arrhenius integral. In addition, the current testing utilized heparinized blood for the purpose of easy sample maintenance, which might adversely have protracted the time required to achieve the complete hemostasis possibly by 2 to 10 times longer, in comparison with a nonheparinized blood sample.<sup>8</sup> Furthermore, the current study used transparent media (i.e., degassed pure water) for PAI to minimize any optical scattering effects that could accompany weak signal generation with low image contrast, lateral distribution of photons, and shallow depth for volumetric imaging. Thus, *in vivo* dorsal chambers in a rat model will be used to examine any biochemical and optical scattering effects of vascularized samples on the coagulation process as well as image reconstruction at various wavelengths. Finally, the ultimate research goal is to develop a portable image-guided HIFU system for rapid hemostasis with minimal collateral damage to tissue. Further investigations will continue to focus on design and development of a rechargeable MOSFET-based RF amplifier with a hand-held HIFU transducer that can be compatible with an optical or ultrasound imaging system.

## 5 Conclusion

The current study presented the feasible application of HFU for thermal hemostasis assisted by visualization of the nonionizing PAI modality under *ex vivo* conditions. Acoustic energy was successfully applied to achieve complete hemostasis in artery along with minimal damage to the peripheral tissue. PAI was able to provide information on the location of HIFU-treated lesions, indicating the great potential to provide feedback on HIFU thermal treatment. The systematic integration of PAI and HIFU will be conducted to achieve the real-time monitoring of the hemostasis process on the injured blood vessels *in vivo*. The proposed technique can be a feasible tool to facilitate blood coagulation and ensure the safety of HIFU treatment with a portable system.

## Acknowledgments

This research was supported by Basic Science Research Program through the National Research Foundation of Korea (NRF) funded by the Ministry of Education, Science and Technology (NRF-2012R1A1A1012965). The authors would like to appreciate Mr. Trung Hau Nguyen for his help on discussion.

## References

1. J. K. Barton, D. P. Popok, and J. F. Black, "Thermal analysis of blood undergoing laser photocoagulation," *IEEE J. Sel. Top. Quantum Electron.* **7**(6), 936–943 (2001).
2. R. R. Krueger and E. E. Almquist, "Argon laser coagulation of blood for the anastomosis of small vessels," *Lasers Surg. Med.* **5**(1), 55–60 (1985).
3. R. E. Rumbaut, Platelet-vessel wall interactions in hemostasis and thrombosis, Morgan & Claypool Publishers LLC, San Rafael, California (2010).
4. S. Vaezy et al., "Liver hemostasis with high-intensity ultrasound: repair and healing," *J. Ultrasound Med.* **23**(2), 217–225 (2004).
5. S. Vaezy and V. Zderic, "Hemorrhage control using high intensity focused ultrasound," *Int. J. Hyperthermia* **23**(2), 203–211 (2007).
6. U. Maestroni et al., "High-intensity focused ultrasound for prostate cancer: long-term follow up and complications rate," *Adv. Urol.* **2012**, 1–4 (2012).

7. R. Ramanathan and R. J. Leveillee, "Ablative therapies for renal tumors," *Ther. Adv. Urol.* **2**(2), 51–68 (2010).
8. S. Vaezy et al., "Use of high-intensity focused ultrasound to control bleeding," *J. Vasc. Surg.* **29**(3), 533–542 (1999).
9. Y. Zhou, "Generation of uniform lesions in high intensity focused ultrasound ablation," *Ultrasonics* **53**(2), 495–505 (2013).
10. J. E. Kennedy, "High-intensity focused ultrasound in the treatment of solid tumours," *Nat. Rev.* **5**(4), 321–327 (2005).
11. E. R. Cordeiro et al., "High-intensity focused ultrasound (HIFU) for definitive treatment of prostate cancer," *BJU Int.* **110**(9), 1228–1242 (2012).
12. A. Burgess et al., "High-intensity focused ultrasound (HIFU) for dissolution of clots in a rabbit model of embolic stroke," *PLoS One* **7**(8), e42311 (2012).
13. C. Wright, K. Hynynen, and D. Goertz, "In vitro and in vivo high-intensity focused ultrasound thrombolysis," *Investig. Radiol.* **47**(4), 217–225 (2012).
14. M. R. Pfeffer et al., "Image-guided high-intensity focused ultrasound in the treatment of cancer," in *Image-Guided Cancer Therapy*, D. E. Dupuy, Y. Fong, and W. N. McMullen, Eds., pp. 79–99, Springer, New York (2013).
15. B. E. O'Neill et al., "MRI-based prediction of pulsed high-intensity focused ultrasound effect on tissue transport in rabbit muscle," *J. Magn. Reson. Imaging* **38**(5), 1094–1102 (2013).
16. R. W. Martin et al., "Hemostasis of punctured vessels using Doppler-guided high-intensity ultrasound," *Ultrasound Med. Biol.* **25**(6), 985–990 (1999).
17. S. Vaezy et al., "Real-time visualization of high-intensity focused ultrasound treatment using ultrasound imaging," *Ultrasound Med. Biol.* **27**(1), 33–42 (2001).
18. C. L. Bayer, G. P. Luke, and S. Y. Emelianov, "Photoacoustic imaging for medical diagnostics," *Acoustics Today* **8**(4), 15–23 (2012).
19. S. Mallidi, G. P. Luke, and S. Emelianov, "Photoacoustic imaging in cancer detection, diagnosis, and treatment guidance," *Trends Biotechnol.* **29**(5), 213–221 (2011).
20. C. Kim, C. Favazza, and L. V. Wang, "In vivo photoacoustic tomography of chemicals: high-resolution functional and molecular optical imaging at new depths," *Chem. Rev.* **110**(5), 2756–2782 (2010).
21. C. Kim et al., "In vivo molecular photoacoustic tomography of melanomas targeted by bioconjugated gold nanocages," *ACS Nano* **4**(8), 4559–4564 (2010).
22. G. Ku and L. V. Wang, "Deeply penetrating photoacoustic tomography in biological tissues enhanced with an optical contrast agent," *Opt. Lett.* **30**(5), 507–509 (2005).
23. K. H. Song and L. V. Wang, "Deep reflection-mode photoacoustic imaging of biological tissue," *J. Biomed. Opt.* **12**(6), 060503 (2007).
24. P. V. Chitnis et al., "Feasibility of optoacoustic visualization of high-intensity focused ultrasound-induced thermal lesions in live tissue," *J. Biomed. Opt.* **15**(2), 021313 (2010).
25. T. Neumann and H. Ermert, "Schlieren visualization of ultrasonic wave fields with high spatial resolution," *Ultrasonics* **44**(Suppl. 0), e1561–e1566 (2006).
26. J. L. Su et al., "Photoacoustic imaging of prostate brachytherapy seeds," *Biomed. Opt. Express* **2**(8), 2243–2254 (2011).
27. L. Faqi et al., "Measuring temperature rise in phantom to determine high power high-intensity focused ultrasound sound field," in *Fourth Int. Conf. Bioinformatics and Biomedical Engineering*, pp. 1–4 (2010).
28. M. Solovchuk, T. W. Sheu, and M. Thiriet, "Simulation of nonlinear Westervelt equation for the investigation of acoustic streaming and nonlinear propagation effects," *J. Acoust. Soc. Am.* **134**(5), 3931–3942 (2013).
29. R. L. Clarke and G. R. ter Haar, "Temperature rise recorded during lesion formation by high-intensity focused ultrasound," *Ultrasound Med. Biol.* **23**(2), 299–306 (1997).
30. M. H. Niemz, *Laser-Tissue Interactions Fundamental and Applications*, 3rd ed., Springer-Verlag, Berlin Heidelberg, New York (1996).
31. S. Vaezy et al., "Hemostasis using high intensity focused ultrasound," *Eur. J. Ultrasound* **9**(1), 79–87 (1999).
32. <http://fieldp.com/myblog/2008/arrhenius-rate-integrals-in-computer-thermal-solutions/>.

33. N. I. Inc., [http://www.newageindustries.com/downloads/catalogs/NewAge\\_Silicone\\_Catalog.pdf](http://www.newageindustries.com/downloads/catalogs/NewAge_Silicone_Catalog.pdf).
34. T. Khamdaeng et al., "Arterial stiffness identification of the human carotid artery using the stress-strain relationship in vivo," *Ultrasonics* **52**(3), 402–411 (2012).
35. I. V. Larina, K. V. Larin, and R. O. Esenaliev, "Real-time optoacoustic monitoring of temperature in tissues," *J. Phys. D* **38**(15), 2633–2639 (2005).
36. B. Soroushian, W. M. Whelan, and M. C. Kolios, "Assessment of opto-mechanical behavior of biological samples by interferometry," *Proc. SPIE* **7177**, 71771X (2009).
37. B. Cox et al., "Quantitative spectroscopic photoacoustic imaging: a review," *J. Biomed. Opt.* **17**(6), 061202 (2012).
38. J. K. Barton et al., "Cooperative phenomena in two-pulse, two-color laser photocoagulation of cutaneous blood vessels," *Photochem. Photobiol.* **73**(6), 642–650 (2001).
39. Y. Sun and B. O'Neill, "Imaging high-intensity focused ultrasound-induced tissue denaturation by multispectral photoacoustic method: an ex vivo study," *Appl. Opt.* **52**(8), 1764–1770 (2013).
40. W. G. Zijlstra, A. Buursma, and W. P. Meeuwse-van der Roest, "Absorption spectra of human fetal and adult oxyhemoglobin, de-oxy-hemoglobin, carboxyhemoglobin, and methemoglobin," *Clin. Chem.* **37**(9), 1633–1638 (1991).
41. J. J. Xia et al., "Characterizing beef muscles with optical scattering and absorption coefficients in VIS-NIR region," *Meat. Sci.* **75**(1), 78–83 (2007).

**Van Phuc Nguyen** received the master's degree in mechatronics engineering from Pukyong National University, Busan, Republic of Korea, in 2012. He is currently working as a PhD candidate in the Bio-Therapeutics Laboratory under the supervision of professor Hyun Wook Kang. His research interests are developing an integration of high intensity focused ultrasound (HIFU) and photoacoustic imaging system in real-time and mobile applications.

Biographies of the other authors are not available.